Asian Journal of Chemistry; Vol. 36, No. 9 (2024), 2025-2037

ASIAN JOURNAL OF CHEMISTRY

https://doi.org/10.14233/ajchem.2024.32060

Molecular Structure, Spectroscopy, Molecular Docking and ADMET Studies of 2,5-Dimethylbenzaldehyde Semicarbazone as Potent Breast Cancer Agent

S. SUMATHI[1], S. JEYAVIJAYAN[1,*], N. KARTHIK[1], A. KARTHIKEYAN[1], PALANI MURUGAN[2] and V.S. KUNJUMOL[1]

[1]Department of Physics, Kalasalingam Academy of Research and Education, Krishnankoil-626126, India
[2]Department of Physics, Dr. B.R. Ambedkar Institute of Technology, Port Blair-744103, India

*Corresponding author: E-mail: s.jeyavijayan@gmail.com

Received: 30 May 2024; *Accepted*: 1 July 2024; *Published online*: 30 August 2024; AJC-21727

The vibrational wavenumbers of 2,5-dimethylbenzaldehyde semicarbazone (DBS) were compared using the DFT-B3LYP/6-311++G(d,p) method after the FTIR and FT-Raman spectra were measured in the ranges of 4000-400 cm^{-1} and 4000-0 cm^{-1}, respectively. The computed and experimental XRD results were compared with the optimized geometries. The energy gap between the lowest unoccupied molecular orbital (LUMO) and the highest occupied molecular orbital (HOMO) as well as the molecule electrostatic potentials (MEP) has been illustrated using charge density distributions indicative of the biological response. The absorption spectra were generated using time-dependent density functional theory calculations on the same basis set. An investigation of natural bonds has revealed strong electron delocalization whereas the electrical properties of the molecule have been elucidated using the Fukui function and Mulliken charge analysis. Molecular orbital contributions were investigated using densities of states (DOS) spectrum. The docking investigation, which was conducted against the protein 1AQU associated with breast cancer revealed that the largest binding energy was -8.3 kcal/mol. To assess the drug-likeness of the compound, an ADMET analysis has also been conducted and examined. Novel insights on the molecular structure will become possible as a result of these theoretical findings.

Keywords: 2,5-Dimethylbenzaldehyde semicarbazone, DFT, Docking, Breast cancer, ADMET.

INTRODUCTION

The high death rate and increasing incidence of cancer are the major global health problems [1,2]. By 2030, cancer will account for about 15 million fatalities worldwide or one in six deaths overall [3]. Several popular cancer treatments, including radiation, chemotherapy, and surgery, only offer cancer patients temporary relief due to their side effects and recurrence risks [4]. Consequently, creating safe, efficient cancer treatments that are resistant to side effects, minimally harm normal cells and have no adverse consequences is a very challenging issue for modern researchers. Semicarbazone derivatives have demonstrated significant promise in preventing tumor development and metastasis, indicating that their effectiveness in treating breast cancer is growing. These compounds offer a novel approach to the treatment of common and challenging diseases because of their distinct molecular makeup and targeted mechanisms of action [5]. Because of their potential for biological applications including DNA, BSA interaction and anticancer activities, semicarbazones have been the focus of a great deal of experimental and theoretical investigation in recent years [6,7].

A thorough literature reveals that 2,5-dimethylbenzaldehyde semicarbazone (DBS) has not been the subject of any experimental or theoretical investigation. These data have served as the basis for significant theoretical investigations such as spectroscopic studies that use density functional theory (DFT/6-311++G(d,p)) computations to look at the characteristics of DBS. DFT calculations were used to confirm spectroscopic data from experiments, namely FT-Raman and FTIR spectra [8-11]. DFT simulation results that the energetic electron link and Becke's 3 parameter (B3) exchange-correlations perform exceptionally well when the Lee Yang and Parr (LYP) connection functional is applied [12-15]. Time-dependent (TD) electronic transitions were calculated in the gas phase to account for the charge transfer in the molecule using the 6-311++G(d,p)

basis set. The study of lowest unoccupied molecular orbitals (LUMO) and highest occupied molecular orbitals (HOMO) has enabled this. To investigate the reactive regions and electronic transitions of molecules, the DFT/B3LYP has therefore been employed, based on molecular reactivity parameters such as MEP surface analysis and frontier molecular orbital analysis. From the overall DOS spectrum, each border molecular orbital may be described. The global reactivity characteristics [16] for DBS moleucle have also been determined including softness, chemical hardness, electronegativity and electrophilicity index. By observing its natural bond orbitals, the compound's intra- and intermolecular interactions have been determined. The docking investigations on proteins connected to breast cancer have been conducted to verify the anti-breast cancer impact of DBS and the results have shown that DBS is the standard drug for treating breast cancer. The drug-likeness of the molecule has also been assessed by the use of ADMET and pharmacological activities [17].

EXPERIMENTAL

A fine polycrystalline 2,5-dimethylbenzaldehyde semicarbazone (DBS) was supplied by Sigma-Aldrich, U.K. An MCT detector, KBr beam splitter and globar source were installed on a BRUKER IFS 66V model FTIR spectrometer, which was used to get the chemical's FTIR spectrum at room temperature. The spectra observed falls between 4000-400 cm^{-1} at a resolution of ± 1 cm^{-1}. The FT-Raman spectrum was obtained with a computer-interfaced BRUKER IFS 66V type interferometer and the FRA-106 FT-Raman accessories.

Quantum computational details: The ideal parameters were found by quantum chemical density functional calculations at the Becke3-Lee-Yang-Parr (B3LYP) level using a 6-311++G(d,p) basis set and the Gaussian 09 W [18] program package. The structural properties of the DBS was tuned before measuring the vibrational wavenumbers and electrical characteristics. It was possible to determine the vibrational wavenumbers by merging the results of the GAUSSVIEW [19] and VEDA [20] algorithms. Vibrational frequency calculations analyze the thermodynamic functions including vibrational energy, entropy and heat capacity. The electrostatic potential (MEP), HOMO and LUMO energies and reactive sites have all been used to calculate the chemical activity of DBS. Performing NBO calculations is important as it assists in measuring the second order interactions between the empty orbitals of one subsystem and the filled orbitals of another, which allows for a better understanding of intermolecular delocalization. GaussSum software [21] was also used to construct DOS spectra in addition to these calculations.

Molecular docking: A computer-based molecular modeling approach was used to assess the inhibitory efficacy of DBS against breast cancer marker proteins. Human progesterone (PDB ID: 1A28), epidermal growth factor (PDB ID: 1M17), estrogen (PDB ID: 1ERE) and estrogen sulfotransferase (PDB ID: 1AQU) receptors are some of the ligand and protein markers utilized with DBS to detect breast cancer. Using PyMOL molecular graphical system [22] (version 1.7.4.5 Edu), the protein-ligand binding position was shown and Auto Dock Vina [23] (version: 4.2.1) was used for the molecular docking. Discovery Studio [24] (version: 2017 R2 client) was used to evaluate the protein structure and amino acid locations prior to molecular docking. The structure of the ligand DBS [25] has been extracted using PubChem, one of the publicly available ligand databases (http://pubchem.ncbi.nlm.nih.gov).

ADMET prediction: The pharmacokinetics and physicochemical properties of the pharmaceutical substance DBS were determined using the pkCSM server [26]. By importing the SMILES of the decanal from the PubChem database into the pkCSM server, the physicochemical and pharmacokinetic parameters such as absorption, aqueous solubility, distribution, metabolism, excretion and toxicity were determined based on the chemical structure of the molecule. The Swiss-ADME web server was then used to execute the boiled-egg model, which resulted in the prediction of several pharmacokinetic properties such as water solubility and drug similarity [27].

RESULTS AND DISCUSSION

Molecular geometry: The DBS numbering system at the DFT/B3LYP level is shown in Fig. 1, which makes use of the optimized structure and the basis set 6-311++G(d,p). The predicted bond lengths and bond angles [28] were compared with X-ray diffraction data from a similar molecule. The predicted geometrical characteristics differ somewhat from those in the single crystal XRD data, as shown in Table-1. The high R^2 value of 0.997 indicates a strong correlation between the regression graph and the observed oscillations. These fluctuations are probably caused by intermolecular interactions in the crystalline state. It was determined that DBS has a global minimum energy of -628.54670236 Hartrees.

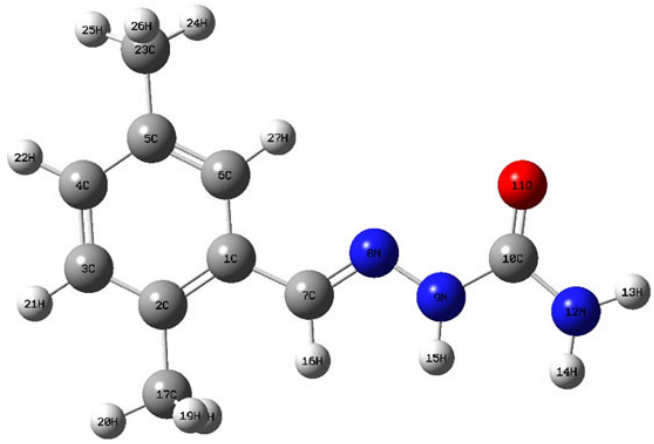

Fig. 1. Optimized structure of 2,5-dimethylbenzaldehyde semicarbazone

Based on the B3LYP/6-311++(d,p) calculation, the bond length of the aromatic ring is found to be as follows: C3–C4 < C5–C6 < C2–C3 \ C4–C5 < C1–C6 < C1–C2. The conjugation between the substituent groups and the ring system clearly caused a major distortion in the typical hexagonal shape of the benzene ring. Inequalities in the ring can also be seen in the bond lengths at the replacement positions, C1–C7, C2–C17 and C5–C23. The computed values for these lengths are 1.467, 1.513 and 1.510 Å (1.461, 1.509 and 1.489 Å by experimental). The

TABLE-1
THE OPTIMIZED STRUCTURAL PARAMETERS OF 2,5-DIMETHYLBENZALDEHYDE SEMICARBAZONE

Bond length (Å)	DFT-B3LYP/6-311++G(d,p)	Exp. [28] R^2 = 0.997	Bond angle (°)	DFT-B3LYP/6-311++G(d,p)	Exp. [28] R^2 = 0.997	Bond angle (°)	DFT-B3LYP/6-311++G(d,p)	Exp. [28] R^2 = 0.997
C1-C2	1.411	1.388	C2-C1-C6	119.7	118.1	N8-N9-C10	120.2	120.0
C1-C6	1.406	1.386	C2-C1-C7	120.6	122.3	N8-N9-H15	119.1	120.9
C1-C7	1.467	1.461	C6-C1-C7	119.7	119.6	C10-N9-H15	118.8	117.8
C2-C3	1.399	1.382	C1-C2-C3	117.9	120.2	N9-C10-O11	124.6	119.1
C2-C17	1.513	1.509	C1-C2-C17	122.7	122.7	N9-C10-N12	111.8	117.4
C3-C4	1.389	1.388	C3-C2-C17	119.4	-	O11-C10-N12	123.6	123.5
C3-H21	1.085	0.930	C2-C3-C4	121.8	121.8	C10-N12-H13	112.7	114.4
C4-C5	1.402	1.373	C2-C3-H21	118.9	119.9	C10-N12-H14	118.6	116.6
C4-H22	1.086	–	C4-C3-H21	119.3	119.1	H13-N12-H14	114.2	127.9
C5-C6	1.390	1.384	C3-C4-C5	120.7	117.5	C2-C17-H18	112.1	–
C5-C23	1.510	1.489	C3-C4-H22	119.5	–	C2-C17-H19	112.1	–
C6-H27	1.084	0.930	C5-C4-H22	119.8	–	C2-C17-H20	110.3	–
C7-N8	1.281	1.275	C4-C5-C6	117.9	121.5	H18-C17-H19	107.4	–
C7-H16	1.095	0.930	C4-C5-C23	120.8	–	H18-C17-H20	107.3	–
N8-N9	1.355	1.377	C6-C5-C23	121.3	–	C19-C17-H20	107.3	–
N9-C10	1.396	1.362	C1-C6-C5	122.0	120.9	C5-C23-H24	111.3	–
N9-H15	1.017	0.930	C1-C6-H27	117.9	119.5	C5-C23-H25	111.1	–
C10-O11	1.209	1.244	C5-C6-H27	120.1	119.5	C5-C23-H26	111.2	–
C10-N12	1.392	1.337	C1-C7-N8	121.9	122.1	H24-C23-H25	107.8	–
N12-H13	1.009	0.935	C1-C7-H16	117.7	118.9	H24-C23-H26	108.0	–
N12-H14	1.010	0.970	N8-C7-H16	120.5	118.9	H25-C23-H26	107.2	–
C17-H18	1.095	–	C7-N8-N9	117.5	115.8			
C17-H19	1.095	–						
C17-H20	1.091	–						
C23-H24	1.091	–						
C23-H25	1.095	–						
C23-H26	1.094	–						

bond angles of C2–C1–C7, C1–C2–C3 and C4–C5–C6 are 120.6º, 117.9º and 117.9º, respectively as determined by DFT calculations (122.3º, 120.2º and 121.5º by experimental). Since, the bond angles increase with electronegativity, these variations are a result of the electronegativity of atoms O11, N8, N9 and N12.

Thermodynamic properties: The calculated thermodynamic parameters for DBS at the DFT/B3LYP/6-311++G(d,p) basis set, which include zero point energy, entropy and heat capacity, are displayed in Table-2. Based on Table-2, the DBS molecule has a total dipole moment of 4.746 Debye. According to simulations, there is a large range in zero-point vibrational energy (ZPVEs), with variations ranging from 137.779 kcal mol^{-1}. The stronger behaviour of DBS in the molecular interaction is shown by the thermodynamic parameters having a bigger value. Furthermore, Table-2 presents the variations in the overall entropy of molecule (122.408 cal mol^{-1} k^{-1}) and its total vibrational energy (146.883 kcal mol^{-1}) at room temperature. The orientations of chemical processes and various thermodynamic energies can be calculated by using the thermodynamic relationships.

Vibrational analysis: The 27 atoms in DBS have a total of 75 common modes of vibration. The DFT/B3LYP/6-311++G(d,p) approach was used to provide the precise vibrational assignments for the molecule. The combined impacts of electron correlation effects and basis set faults lead to computed frequencies that are greater than the corresponding experimental frequencies. Here, the B3LYP technique's scale factor [29] of 0.9613 helps

TABLE-2
THE THERMODYNAMIC PARAMETERS OF 2,5-DIMETHYLBENZALDEHYDE SEMICARBAZONE

Parameters	DFT-B3LYP/6-311++G(d,p)
Optimized global minimum energy (Hartrees)	-628.54670236
Total energy (thermal), E_{total} (kcal mol^{-1})	146.883
Heat capacity, C_v (cal mol^{-1} k^{-1})	53.290
Total entropy, S (cal mol^{-1} k^{-1})	122.408
Translational entropy (cal mol^{-1} k^{-1})	41.649
Rotational entropy (cal mol^{-1} k^{-1})	32.442
Vibrational entropy (cal mol^{-1} k^{-1})	48.318
Vibrational energy, E_{vib} (kcal mol^{-1})	145.105
Zero-point vibrational energy, (kcal mol^{-1})	137.779
Rotational constants (GHz)	
A	1.244
B	0.317
C	0.254
Dipole moment (Debye)	4.746

in making sure the calculated wavenumbers are scaled appropriately. The vibrational frequencies of molecules derived by theoretical and experimental methods (FTIR and FT-Raman) are compared in Table-3 and its spectra are displayed in Fig. 2.

C-H vibrations: In the range of 3100-3000 cm^{-1}, aromatic compounds usually exhibit a large number of weak bands due to their C-H stretching vibrations [30]. Consequently, the Raman bands found at 3065, 3030, 3005 and 2990 cm^{-1} in DBS and the infrared bands seen at 3060, 3017, 3000 and 2992 cm^{-1} have

TABLE-3
THE VIBRATIONAL ASSIGNMENTS BASED ON PED CALCULATIONS FOR 2,5-DIMETHYLBENZALDEHYDE SEMICARBAZONE

S. No.	Observed wavenumber (cm^{-1})		Wavenumber (cm^{-1})		IR intensity (Km mol^{-1})	Raman activity (Å^4 amu^{-1})	Assignment with PED (%)
	FT-IR	FT- Raman	Calculated	Scaled			
1	3542(ms)	3540(w)	3680	3537	39	77	νNH(100)
2	3449(vs)	3430(w)	3569	3431	49	232	NH_2 ass(99)
3	3341(vw)	3340(w)	3480	3345	8	288	NH_2ss(98)
4	3060(vw)	3065(w)	3185	3062	2	39	νCH(96)
5	3017(vw)	3030(w)	3169	3046	28	215	νCH(94)
6	3000(w)	3005(w)	3151	3029	10	77	νCH(91)
7	2992(w)	2990(w)	3106	2986	13	48	νCH(90)
8	2982(w)	2984(w)	3102	2982	20	71	CH_3 ips(92)
9	-	2955(w)	3071	2952	18	106	CH_3 ips(89)
10	2950(s)	2943(w)	3065	2946	18	71	CH_3 ss(87)
11	-	2925(w)	3039	2922	68	115	CH_3 ss(85)
12	2900(w)	2910(w)	3023	2906	36	289	CH_3 ops(84)
13	-	2895(w)	3018	2901	18	173	CH_3 ops(82)
14	1725(vs)	1731(w)	1804	1734	410	51	νC=O(81)
15	-	1609(vs)	1674	1610	3	767	NH_2sciss(80)
16	-	1577(vs)	1642	1579	2	1224	νC=N(70)
17	1581(vs)	1560(w)	1629	1566	136	83	νCC(83)
18	1550(ms)	1550(w)	1605	1543	15	74	νCC(86)
19	1480(vs)	1499(w)	1554	1494	384	46	νCC(84)
20	1461(ms)	1465(vw)	1527	1467	66	3	νCC(81)
21	-	1451(vw)	1505	1447	25	17	νCC(85)
22	-	1431(vw)	1493	1435	4	11	νCC(80)
23	-	1428(vw)	1492	1434	8	10	CH_3 ipb(78)
24	1400(w)	-	1488	1431	6	10	CH_3 ipb(79)
25	1398(w)	1381(s)	1438	1382	5	128	CH_3 sb (77)
26	-	1363(vw)	1416	1361	2	21	CH_3sb (73)
27	-	1359(vw)	1415	1360	1	12	νCC (76)
28	1350(ms)	1340(s)	1395	1341	48	32	νCC (74)
29	1270(vw)	1275(s)	1325	1274	5	46	νCC (75)
30	-	1250(s)	1310	1259	3	88	bNH(72)
31	1256(ms)	-	1300	1249	427	21	νNN(71)
32	-	1252(ms)	1266	1217	21	204	νCN(70)
33		1170(w)	1225	1178	0	69	νCN(70)
34	1154(ms)	1150(vw)	1190	1144	50	12	CH_3 opb(69)
35	1100(ms)	1120(ms)	1177	1131	194	125	CH_3 opb(67)
36	1073(ms)	-	1123	1079	86	34	CH_3opr(65)
37		1052(w)	1086	1044	48	40	CH_3opr(66)
38	1000(vw)	-	1066	1024	5	0	bCH (68)
39	-	982(vw)	1056	1015	0	2	bCH (67)
40	990(vw)	-	1039	999	2	7	bCH (62)
41	985(vw)	981(w)	1024	984	1	30	NH_2 rock(60)
42	965(ms)	960(vw)	1000	961	10	4	bCH (64)
43	931(vw)	-	972	934	3	0	CH_3 ipr(65)
44	900(vw)	920(vw)	954	917	11	7	ωNH(60)
45	-	902(w)	948	911	5	35	CH_3 ipr(65)
46	880(vw)	-	923	888	3	0	Rasymd(66)
47	780(ms)	793(vw)	824	792	24	1	Rsymd(68)
48	765(vw)	772(w)	806	775	3	23	Rtrigd(65)
49	-	735(vw)	760	731	29	3	bCC(69)
50	-	710(vw)	733	705	2	2	bCC(67)
51	700(vw)	703(vw)	732	704	2	1	bCC(66)
52	-	653(vw)	693	666	15	3	bC=N(69)
53	-	626(vw)	651	625	1	8	bCN(64)
54	-	550(vw)	577	554	1	1	bCN(64)
55	515(ms)	523(vw)	548	527	230	4	bNN(65)
56	509(ms)	500(vw)	536	516	30	2	ωCH(58)
57	-	460(vw)	482	464	18	8	ωCH(60)
58	450(ms)	451(vw)	473	455	19	1	ωCH(59)
59	-	448(vw)	468	450	16	12	ωCH(58)

60	420(ms)	405(vw)	451	434	48	11	NH_2 wag(66)
61	412(vw)	-	386	371	5	0	ωC=N(59)
62	-	351(vw)	366	352	46	3	ωCN(63)
63	-	325(vw)	337	324	2	2	ωCN(63)
64	-	305(vw)	323	311	0	1	bC=O(67)
65	-	265(vw)	287	276	1	1	ωCC(60)
66	-	227(vw)	241	231	0	2	ωCC(59)
67	-	185(vw)	198	190	6	3	ωCC(60)
68	-	169(vw)	182	175	14	3	ωC=O(57)
69	-	150(vw)	150	145	1	1	tRasymd(55)
70	-	125(vw)	136	130	1	1	ωNN(54)
71	-	100(vw)	114	109	4	1	tRsymd(58)
72	-	60(vw)	66	63	6	2	tRtrigd(60)
73	-	53(vw)	58	56	6	1	NH_2 twist(56)
74	-	41(vw)	50	48	0	1	tCH_3(55)
75	-	25(vw)	31	30	11	1	tCH_3(54)

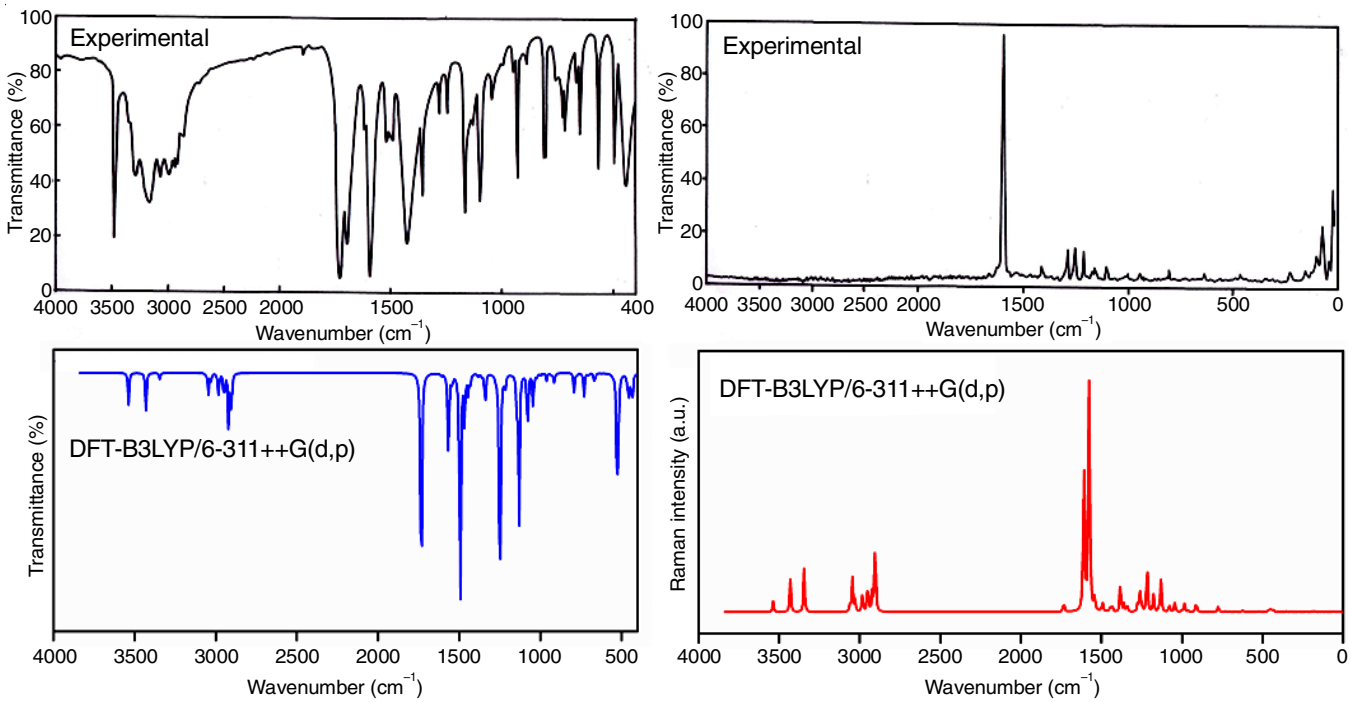

Fig. 2. FTIR and FT-Raman spectra of 2,5-dimethylbenzaldehyde semicarbazone

been linked to the C-H stretching vibrations. These assignments are further supported by the PED values of these modes, which exceed 90%. Sharp bands are generally observed as a result of the interaction between C-H in-plane bending vibrations and C-C stretching vibrations in the 1300-1000 cm^{-1} range. In this work, the infrared bands at 1000, 990 and 965 cm^{-1} and the FT-Raman bands at 982 and 960 cm^{-1} are attributed to C-H in-plane bending vibrations. The strongly coupled out-of-plane C-H bending vibrations are located in the range 900-667 cm^{-1}. Furthermore, the out-of-plane C-H bending vibrations for molecules have been identified and are displayed in Table-3. For the C-H vibrational modes, there is excellent agreement between the observed and B3LYP calculated values.

CH_3 vibrations: In aromatic ring systems, the ring usually receives electrons from the vibrations of the CH_3 group. The regions at 2980 and 2870 cm^{-1} are due to the symmetric and antisymmetric stretching modes of CH_3 group [31], respectively. The vibrational bands at 2982, 2984 and 2955 cm^{-1} are attributed to the CH_3 in-plane stretching mode of vibrations, which accounts for over 90% of the PED, because of the two methyl groups found in DBS. The bands at 2950, 2943 and 2925 cm^{-1} are thought to be the result of symmetric stretching of CH_3. The bands at 2900, 2910 and 2895 cm^{-1} are thought to be responsible for out-of-plane CH_3 stretching. For derivatives substituted with methyl [31], the symmetric and antisymmetric deformation modes of the CH_3 group frequently occur in the ranges of 1390-1370 cm^{-1} and 1465-1440 cm^{-1}, respectively. Moreover, the bands at 1428 and 1400 cm^{-1} in the molecule are ascribed to the in-plane CH_3 bending modes of vibrations, whereas the bands at 1398, 1381 and 1363 cm^{-1} are assigned to the symmetric CH_3 bending. The other modes of vibration of the CH_3 group are shown in Table-3 and also exhibit a strong agreement with the wavenumbers obtained by using the B3LYP/6-311++G(d,p).

C-C and C-N vibrations: The Raman and reported IR spectra exhibit characteristic bands at 1600 and 1400 cm^{-1}, which can be attributed to aromatic C-C stretching vibrations [32]. The FTIR at 1581, 1550, 1480, 1461, 1350 and 1270 cm^{-1} and the FT-Raman spectrum at 1560, 1550, 1499, 1465, 1451, 1431, 1359, 1340 and 1275 cm^{-1} thus support the C-C stretching vibrations, which are further substantiated by the PED% of DBS. The ring vibrational modes are influenced by the functional groups present in the molecular ring. The possibility of many bands in the region mixing makes it challenging to distinguish between C=N and C–N vibrations. According to Karabacak *et al.* [33], the FTIR spectra at 1689 and 1302 cm^{-1}, respectively, have been assigned to C=N and C–N stretching. The C=N and C–N vibrations in this experiment are detected in Raman at 1577 and 1252, 1170 cm^{-1}. Bending vibrations of the C-N were detected in FTIR at 515 cm^{-1} and in FT-Raman at 626, 550 and 523 cm^{-1}. The vibrational spectrum showed the C-N out-of-bending vibrations at 412, 351 and 325 cm^{-1}.

NH_2 vibrations: The two stretching vibrations (symmetric and asymmetric stretching modes) and the four bending vibrations (twisted, rocking, wagging and scissoring) comprise the six normal modes of the amino group. The N-H stretching vibrations in primary amines generally occur in the range [34] of 3500-3300 cm^{-1}. The FT-Raman indicates 3430 cm^{-1} for the asymmetric stretching vibration of DBS, while the FTIR spectrum displays a highly significant peak at 3449 cm^{-1}. The symmetric stretching vibration of the NH_2 group in the FT-Raman and FTIR spectra is indicated by two bands: one at 3341 cm^{-1} and the other at 3340 cm^{-1}. They can both be considered pure N-H stretching, since nearly all of these modes are seen in the PED data. The scissoring mode for NH_2 groups frequently occurs within the range of 1650-1615 cm^{-1}. The NH_2 scissoring mode is matched by an extraordinarily strong band in FT-Raman at 1609 cm^{-1}. The fact that the PED contributed 80% of this peak provides more support for the conclusions. A remarkably weak bands at 985 and 981 cm^{-1} (60% PED) has been recognized as the NH_2 rocking vibration; this result closely aligns with the scaled value of 984 cm^{-1}. The wagging mode of the NH_2 group is responsible for the bands located at 420 and 405 cm^{-1} in the vibrational spectrum. Twisting mode of NH_2 group is identified as an extremely faint band at 41 cm^{-1} in FT-Raman.

HOMO-LUMO and DOS spectrum analysis: The stability of the structure is shown by the energy gap of the frontier molecular orbital (FMO). In addition, the FMOs reveal the kinetic stability and chemical reactivity of the molecule. It can assist in identifying the most reactive areas of a molecule and found that the HOMO and LUMO orbitals the will have energies of -6.10 and -1.63 eV, respectively. The energy gap of the molecule ($\Delta E_{HOMO} - E_{LUMO}$) was found to be 4.47 eV. Softness is shown by a wide energy gap, which is linked to low stability and high chemical reactivity, while good stability and low chemical reactivity are indicated by a small energy gap. The molecule under investigation has lower values of the HOMO and LUMO energy gaps, which suggests that it is highly polarizable, biologically active and chemically reactive. The frontier molecular orbital dispersion of the DBS molecule is displayed in Fig. 3. Moreover, Table-4 displays the calculation results for the global reactivity parameters, which include global softness (S), chemical potential (μ), electrophilicity index (ω) and global hardness (η). For DBS, the calculated values of chemical potential, chemical hardness, chemical softness and electrophilicity index are -3.87 eV, 2.24 eV, 0.22 eV^{-1} and 3.34 eV, respectively.

It is possible for neighbouring orbitals to have the same degenerate energy levels in a border zone, which might not be acceptable to characterize border orbitals using only HOMO and LUMO. As such, the density of states (DOS) is equivalent to the total of the electron densities of states for alpha (α) and

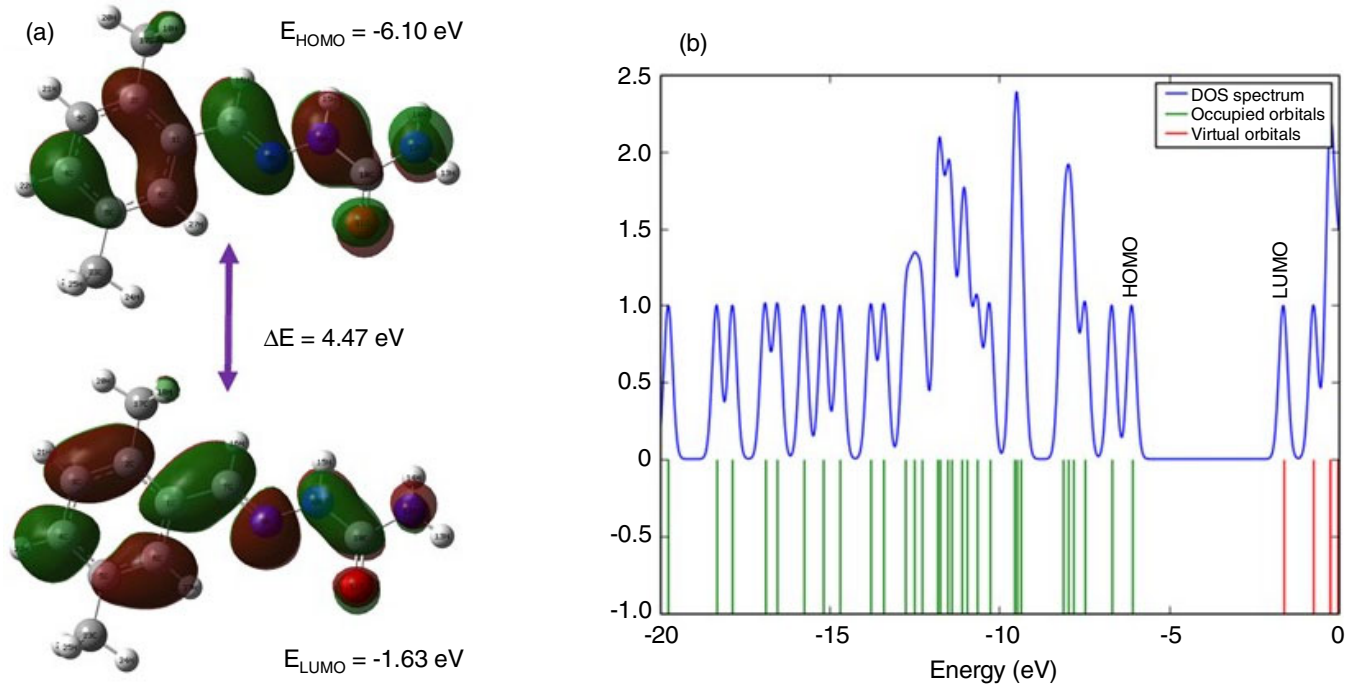

Fig. 3. (a) HOMO-LUMO and (b) DOS spectrum of 2,5-dimethylbenzaldehyde semicarbazone

TABLE-4
GLOBAL REACTIVITY DESCRIPTORS FOR
2,5-DIMETHYLBENZALDEHYDE SEMICARBAZONE

Molecular properties	B3LYP/6-311++G(d,p)
HOMO (eV)	-6.10
LUMO (eV)	-1.63
ΔE ($E_{HOMO} - E_{LUMO}$) (eV)	4.47
Ionization potential (I) (eV)	6.10
Electron affinity (A) (eV)	1.63
Global hardness (η) (eV)	2.24
Global softness (S) (eV^{-1})	0.22
Electronegativity (χ) (eV)	3.87
Chemical potential (μ) (eV)	-3.87
Global electrophilicity (ω) (eV)	3.34

beta (β) [35]. These are generated by employing the GaussSum 3.0 program [36] to combine Gaussian curves with the molecular orbital data. The impact of DBS's orbital arrangement on the chemical bonds that bind its atoms together is depicted in Fig. 3. The density of states graphic illustrates the composition of the energy gap and the orbitals at the system's boundary. For DBS, which has 51α and 51β electrons respectively, DOS is occupied by 102 electrons overall.

Molecular electrostatic potential: The theoretical concept of molecular electrostatic potential is commonly utilized to study electrophilic, nucleophilic and hydrogen bonding sites [37]. The MEP surfaces of DBS at the B3LYP/6-311++G(d,p) technique are shown in Fig. 4. Molecule reactivity can be predicted visually by observing different colours, which represent different MEP values and magnitudes. The colour red denotes the greatest electronegative potential or strong repulsion, whereas the colour blue denotes the highest positive region, or strong attraction. Areas that are tinted green often represent a neutral potential [38]. In the following order, electrostatic potential rises gradually from negative to positive: red < orange < yellow < green < blue. The semicarbazone branching region

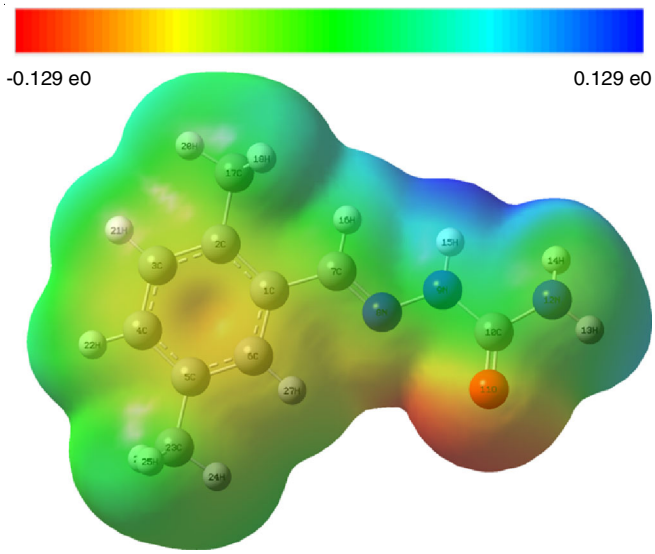

Fig. 4. MEP plot of 2,5-dimethylbenzaldehyde semicarbazone

in the MEP diagram of DBS is linked to the highest negative regions, which are primarily over the O11 atom. MEP demonstrated the highest positive regions in case of a positive potential are above hydrogen atoms. The benzaldehyde semicarbazone moiety of the O-alkylated isomer is therefore shown to have outstanding electrical characteristics with a broad spectrum of electrophilic and nucleophilic sites, which these results both confirm and strengthen.

Natural bond orbital analysis: NBO analysis has been used to investigate the donor-acceptor interactions. Table-5 presents the findings from the NBO study for DBS using the DFT/B3LYP/6-311++G(d,p) basis set. In NBO analysis, stronger system conjugation and a higher probability of donors giving to acceptors are generally indicated by the greatest value of E(2). The orbitals that have the highest stabilization energies in DBS

TABLE-5
SECOND-ORDER PERTURBATION THEORY ANALYSIS OF FOCK MATRIX
FOR 2,5-DIMETHYLBENZALDEHYDE SEMICARBAZONE

Donor(i)	ED (i) (e)	Acceptor (j)	ED (j) (e)	Stabilization energy E(2) (Kcal/mol)	Energy difference E(j) –E(i) (arb. units)	Fock matrix element F(i,j) (arb. units)
π(C1-C2)	1.629	π^*(C3-C4)	0.326	19.30	0.28	0.07
π(C1-C2)	1.629	π^*(C5-C6)	0.303	18.57	0.29	0.07
π(C1-C2)	1.629	π^*(C7-N8)	0.191	18.76	0.25	0.06
π(C3-C4)	1.681	π^*(C1-C2)	0.396	20.10	0.29	0.07
π(C3-C4)	1.681	π^*(C5-C6)	0.303	18.74	0.30	0.07
π(C5-C6)	1.657	π^*(C1-C2)	0.396	20.37	0.28	0.07
π(C5-C6)	1.657	π^*(C3-C4)	0.326	20.65	0.28	0.07
π(C7-N8)	1.936	π^*(C1-C2)	0.396	8.67	0.38	0.06
LP(1)N8	1.911	σ^*(C7-H16)	0.036	9.98	0.76	0.08
LP(1)N8	1.911	σ^*(N9-H15)	0.040	8.95	0.73	0.07
LP(1)N9	1.713	π^*(C7-N8)	0.191	27.33	0.30	0.08
LP(1)N9	1.713	π^*(C10-O11)	0.309	42.28	0.35	0.11
LP(2)O11	1.840	σ^*(N9-C10)	0.090	27.73	0.65	0.12
LP(2)O11	1.840	σ^*(C10-N12)	0.072	25.08	0.65	0.12
LP(1)N12	1.834	π^*(C10-O11)	0.309	25.97	0.37	0.09
π^*(C3-C4)	0.326	π^*(C5-C6)	0.303	210.55	0.01	0.08
π^*(C7-N8)	0.191	π^*(C1-C2)	0.396	50.90	0.03	0.07
π^*(C10-O11)	0.309	σ^*(C10-O11)	0.038	10.46	0.52	0.16

are π(C–C2)→π*(C3–C4), π(C1–C2)→π*(C–C6), π(C1–C2) →π*(C7–N8), π(C3–C4)→π*(C1–C2), π(C3–C4)→π*(C5–C6), π(C5–C6)→π*(C1–C2) and π(C5–C6)→π*(C3–C4) (19.30, 18.57, 18.76, 20.10, 18.74, 20.37 and 20.65 kcal mol^{-1}) orbitals. The stabilization energies of 42.28 and 27.73 kcal mol^{-1} are obtained by the lone pair nitrogen and oxygen with the antibonding orbitals σ*(C10-O11) and σ*(N9-C10), indicating a significant delocalization. It is demonstrated that the antibonding orbitals π*(C3–C4)→π*(C5–C6) and π*(C7–N8)→ π*(C1–C2) in DBS exhibit superior intramolecular interaction, with maximal stabilization energies of 210.55 and 50.90 kcal mol^{-1}, respectively. The presence of these interactions within the molecule is indicative of more advanced biological activity.

Mulliken's population analysis: Fig. 5 shows the charge distribution in DBS using B3LYP and the 6-311++G(d,p) basis set. Table-6 presents the findings when amino and methyl groups are substituted in the aromatic ring, there is a redistribution of electron density and revealed that the charge density at C2 was higher compared to the other carbon atoms in the ring. The significant positive charge at C2 is caused by the influence of the methyl group attached to C2. The atom N12 in DBS has a higher negative charge (-0.321) than the other nitrogens. Moreover, there have been negative reactive reactions involving the nitrogen atoms N8 (-0.043), N12 (-0.321) and O11 (-0.356). All of the carbon atoms with negative charges are C3 (-0.706), C4 (-0.067), C6 (-0.999), C7 (-0.318), C17 (-0.673) and C23 (-0.522). These arise from the increased electronegativity of oxygen and nitrogen atoms linked by a carbon bond and all hydrogen in DBS has a positive charge.

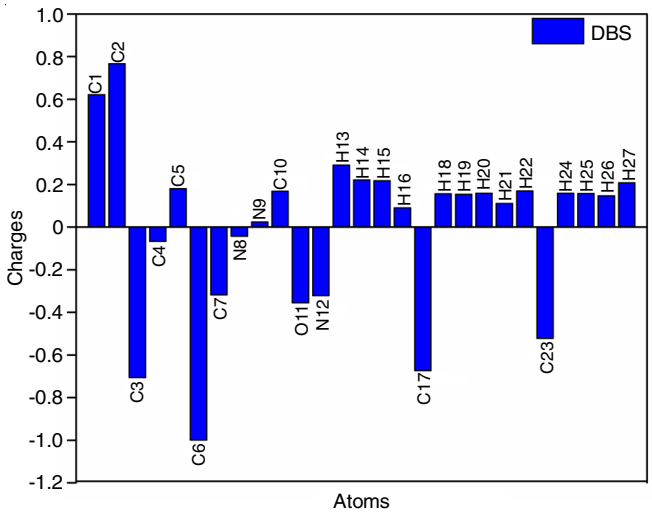

Fig. 5. Mulliken charges plot of 2,5-dimethylbenzaldehyde semicarbazone

TABLE-6
MULLIKEN ATOMIC CHARGES FOR
2,5-DIMETHYLBENZALDEHYDE SEMICARBAZONE

Atoms	Atomic charges (Mulliken) by B3LYP/6-311++G(d,p)	Atoms	Atomic charges (Mulliken) by B3LYP/6-311++G(d,p)
C1	0.621	H15	0.218
C2	0.766	H16	0.090
C3	-0.706	C17	-0.673
C4	-0.067	H18	0.157
C5	0.181	H19	0.154
C6	-0.999	H20	0.159
C7	-0.318	H21	0.111
N8	-0.043	H22	0.170
N9	0.024	C23	-0.522
C10	0.169	H24	0.159
O11	-0.356	H25	0.157
N12	-0.321	H26	0.147
H13	0.291	H27	0.208
H14	0.221		

Fukui function: The Fukui function and the local softness are two additional local reactivity parameters that are needed in addition to the global features to address the reactive behaviour of the atoms in building molecules in different ways. The fukui function also referred to as the frontier function is used to predict the reactivity sites of molecules and to detect nucleophilic and electrophilic assaults, respectively. The condensed form of the Fukui function is stated as for an atom k in a molecule [39, 40].

$$f_k^+ = q_j(N+1) - q_j(N)$$

$$f_k^- = q_j(N) - q_j(N-1)$$

$$f_k^0 = \frac{1}{2}\left[q_j(n+1) - q_j(N-1)\right]$$

These are the DBS groups that are electrophilic, nucleophilic and free radicals. In case of neutral (N), anionic (N+1) and cationic (N-1) chemical species, the atomic charge at the j^{th} site is denoted by the symbol q_j. A dual descriptor, defined as the difference between the nucleophilic and electrophilic functions [41] and can represented as follows:

$$\Delta f(r) = f_k^+ - f_k^-$$

All the three equations above were used to define the Fukui function, which determines the pin point distribution of the atomic sites on the molecule by evaluating the reactivity at atomic resolution. Here, Mulliken population analysis was used to determine the fukui function of DBS at the B3LYP/6-311++ G(d,p) basis set. The dual descriptor employs their sign in a specific location to discriminate between electrophilic and nucleophilic assaults. C1, C2, C5, C17, C23, O11, N9, N12, H14, H20, H21, H22, H24 and H27 are the nucleophilic sites for DBS that meet the requirements of the dual descriptor based on the values as displayed in Table-7. In contrast, B3LYP/6-311++G(d,p) basis set have negative values for the electrophilic sites C3, C4, C6, C7, N8, C10, H13, H15, H16, H18, H19, H25 and H26. Depending on its local behaviour during the process, the molecule DBS responds to both electrophilic and nucleophilic assaults.

Molecular docking: The DBS docking simulations have involved the selection of human progesterone and estrogen receptors based on previous research findings [42,43]. The receptors for human progesterone (PDB ID: 1A28, 4OAR), human estrogen (PDB ID: 1ERE), human growth factor (PDB ID: 1M17) and estrogen sulfotransferase (PDB ID: 1AQU) are among the proteins. These proteins have been shown to interact with DBS (Figs. 6 and 7 from *in silico* analysis) and the docking scores are shown in Table-8. The target protein was pre-processed to

TABLE-7
FUKUI FUNCTIONS FROM MULLIKEN CHARGES FOR 2,5-DIMETHYLBENZALDEHYDE SEMICARBAZONE

Atoms	In gas phase						
	Mulliken charges			Fukui functions			
	q(N+1)	q(N)	q(N-1)	f_k^+	f_k^-	f_k^0	Δf(r)
C1	0.678	0.621	0.669	0.057	-0.048	0.005	0.104
C2	0.810	0.766	0.760	0.044	0.006	0.025	0.038
C3	-0.714	-0.706	-0.711	-0.007	0.004	-0.001	-0.012
C4	-0.226	-0.067	0.062	-0.159	-0.128	-0.144	-0.031
C5	0.222	0.181	0.144	0.042	0.037	0.039	0.004
C6	-1.069	-0.999	-1.010	-0.070	0.010	-0.030	-0.081
C7	-0.442	-0.318	-0.284	-0.124	-0.034	-0.079	-0.089
N8	-0.253	-0.043	0.098	-0.210	-0.140	-0.175	-0.070
N9	0.144	0.024	0.035	0.120	-0.011	0.054	0.131
C10	0.164	0.169	0.152	-0.004	0.017	0.006	-0.021
O11	-0.415	-0.356	-0.276	-0.059	-0.080	-0.069	0.020
N12	-0.332	-0.321	-0.289	-0.010	-0.032	-0.021	0.022
H13	0.250	0.291	0.323	-0.041	-0.031	-0.036	-0.010
H14	0.202	0.221	0.243	-0.019	-0.021	-0.020	0.002
H15	0.165	0.218	0.268	-0.053	-0.050	-0.051	-0.003
H16	0.030	0.090	0.149	-0.060	-0.059	-0.059	-0.002
C17	-0.666	-0.673	-0.640	0.007	-0.033	-0.013	0.039
H18	0.097	0.157	0.189	-0.060	-0.032	-0.046	-0.028
H19	0.087	0.154	0.185	-0.067	-0.031	-0.049	-0.036
H20	0.125	0.159	0.195	-0.035	-0.036	-0.035	0.001
H21	0.051	0.111	0.171	-0.060	-0.060	-0.060	0.000
H22	0.108	0.170	0.242	-0.062	-0.072	-0.067	0.010
C23	-0.566	-0.522	-0.472	-0.044	-0.050	-0.047	0.006
H24	0.141	0.159	0.184	-0.019	-0.024	-0.021	0.005
H25	0.115	0.157	0.195	-0.042	-0.038	-0.040	-0.004
H26	0.109	0.147	0.181	-0.039	-0.034	-0.036	-0.005
H27	0.183	0.208	0.240	-0.025	-0.032	-0.028	0.007

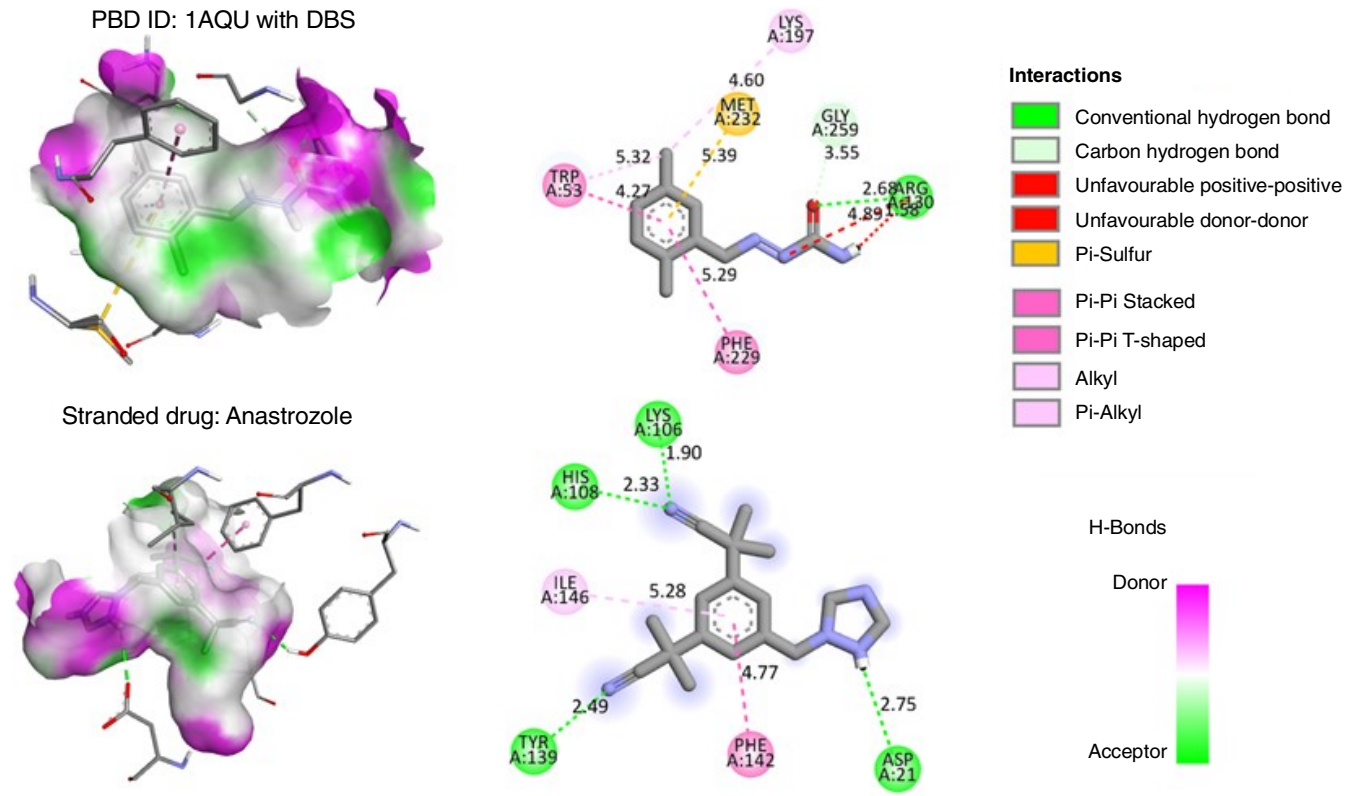

Fig. 6. Molecular docking of 3D and 2D interaction with H-Bond donor-acceptor colour grade for 2,5-dimethylbenzaldehyde semicarbazone with 1AQU target protein and stranded drug anastrozole

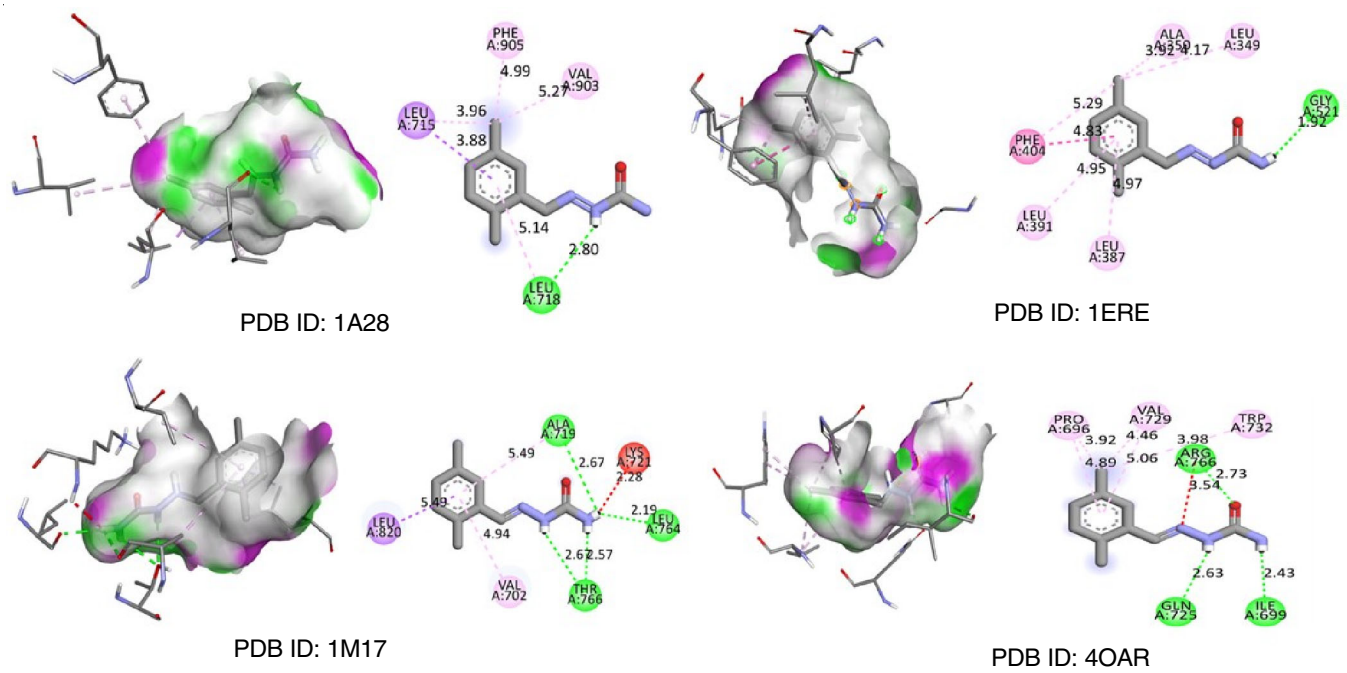

Fig. 7. Molecular docking of 3D and 2D interaction with H-Bond donor-acceptor colour grade for 2,5-dimethylbenzaldehyde semicarbazone with 1A28, 1ERE, 1M17, 4OAR target proteins

TABLE-8
BINDING ENERGIES OF 2,5-DIMETHYLBENZALDEHYDE SEMICARBAZONE WITH BREAST CANCER PROTEIN MARKERS

Protein ID	Binding affinity with DBS kcal/mol)	H-bonding with distance (Å)	Bond type in DBS	Standard anti-breast cancer drugs	Binding affinity with anastrozole (kcal/mol)
1AQU	-8.3	ARG A:130 (2.68 Å)	Conventional HB Carbon HB	Anastrozole	-8.4
1A28	-7.1	LEU A:718 (2.80 Å)	Unfavourable positive-positive Unfavourable donor-donor		-6.4
1ERE	-7.0	GLY A:521 (1.92 Å)	Pi-Sulfur Pi-Pi Stacked		-7.5
1M17	-6.8	ALA A:719 (2.67 Å), LEU A:764 (2.19 Å), THR A:766 (2.67, 2.57 Å)	Pi-Pi T-Shaped Alkyl		-8.2
4OAR	-6.7	AGR A:766 (2.73 Å), ILE A:699 (2.43 Å), GLN A:725 (2.63 Å)	Pi-Alkyl Pi-sigma		-8.0

eliminate ligand groups and water molecules before being transformed into macromolecules by the Autodock vina procedure [44]. Following that the ligand molecule was changed into "pdbqt" by reducing their energies. Table-8 illustrates the results, which show that DBS interacts with the 1AQU receptor in a single conventional hydrogen bond interaction. At 2.68 Å, there is a strong binding between the conventional bond type in DBS and the ARG A:130 residue. With a binding affinity of -8.3 kcal mol^{-1}, these interactions establish the maximum contact between protein 1AQU and DBS. Like THR A: 766 (2.67 Å and 2.57 Å), LEU A:764 (2.19), ALA A:719 (2.67 Å) and ARG A:766 (2.73 Å), GLN A:725 (2.63 Å) and ILE A:699 (2.43 Å), these molecules have three hydrogen bond interactions with DBS for the receptors 1M17 and 4OAR. Their binding affinities are -6.7 kcal mol^{-1} and -6.8 kcal mol^{-1}, respectively. Further analysis revealed that 1ERE and 1A28 held a single conventional hydrogen bond, with GLY A: 521 and LEU A: 718 separated by 1.92 Å and 2.80 Å, respectively. The binding affinities of -7.1 and -7.0 kcal mol^{-1} with DBS are produced by these proteins. Similar to the binding affinity found in this work, anastrozozole, a commonly used drug, has a binding affinity of -8.4 kcal mol^{-1}. DBS is a more successful treatment for breast cancer because of its positive interactions with protein markers.

Pharmacokinetic prediction: The pkCSM server was used in this work to predict a number of pharmacokinetic parameters pertaining to the absorption, distribution, metabolism, excretion and toxicity of the chemical. The DBS pharmacokinetic data are shown in Table-9. There is higher Caco-2 permeability if the log Papp value that the pkCSM server has recorded is greater than 0.90. According to the log Papp 10^{-6} cm/s of 0.714, the molecule is most likely permeable to Caco-2. The human gut is necessary for the absorption of nutrients and medications. Poor intestinal absorption is defined as any drug whose absorption level is less than 30% [45]. In the human stomach, a molecule absorbs 83.372% of its contents. When administered orally, a higher HIA suggests that the medication may be absorbed more quickly. The most difficult challenge in the development of topical medications is getting beyond the skin's protective

TABLE-9
ADMET PROFILE OF 2,5-DIMETHYLBENZALDEHYDE SEMICARBAZONE

	ADMET prediction	DBS
Absorption	CaCo-2 permeability (log Papp in 10^{-6} cm/s)	0.714
	Intestinal absorption (human) (%)	83.372
	Skin permeability (log Kp)	-2.957
	P-glycoprotein substrate	No
	P-glycoprotein I inhibitor	No
	P-glycoprotein II inhibitor	No
Distribution	VDss (human) (log L/kg)	0.02
	Fraction unbound (human) (Fu)	0.435
	BBB permeability (log BB)	-0.331
	CNS permeability (log PS)	-2.364
Metabolism	CYP2D6 substrate	No
	CYP3A4 substrate	No
	CYP1A2 inhibitior	No
	CYP2C19 inhibitior	No
	CYP2C9 inhibitior	No
	CYP2D6 inhibitior	No
	CYP3A4 inhibitior	No

	ADMET prediction	DBS
Excretion	Total clearance (log mL/min/kg)	0.67
	Renal OCT2 substrate	No
	Renal OCT2 substrate	
Toxicity	AMES toxicity test	No
	Max. tolerated dose (human) (log mg/kg/day)	0.941
	hERG I inhibitor	No
	hERG II inhibitor	No
	Oral Rat Acute Toxicity (LD_{50}) (mol/kg)	2.303
	Oral rat chronic toxicity (LOAEL) (log mg/kg_bw/day)	0.954
	Hepatotoxicity	No
	Skin Sensitization	No
	T. pyriformis toxicity (log µg/L)	0.119
	Minnow toxicity (log mM)	2.007

	Pharmacokinetic properties	DBS
Physiochemical properties	Molecular weight (g/mol)	191.23 g/mol
	No. of hydrogen bond acceptors	2
	No. of hydrogen bond donors	2
	Fraction Csp3	0.20
Water solubility	ESOL	-1.98
	ALI	-2.35
	SILICOS-IT	-2.91
Lipophilicity	ILOGP	1.08
	XLOGP3	1.33
	WLOGP	1.31
	MLOGP	1.69
	SILICOS-IT	1.50
Drug likeness	Lipinski	Yes
	Veber	Yes
	Ghose	Yes
	Egan	Yes
	Bioavailability score	0.55

barrier. Several *in silico* techniques are used to evaluate the skin penetration depth of DBS. The logKp value of -2.957 suggests that the molecule has better dermal permeability, according to the statistics provided by the pkCSM server. The whole dosage of a medication that would be dispersed evenly to provide a concentration comparable to blood plasma is known as the hypothetical volume of distribution (VDss). A greater distribution of the medication in tissue compared to plasma is shown by increased VDss. A molecule with a VDss of 0.02 was found, suggesting a significant volume of dispersion.

It implies that the brain can be shielded from dangerous drugs *via* the permeable blood-brain barrier (BBB). If the log BBB is -1, it indicates that the molecule is not well distributed to the brain [46]. However, if the chemical can cross the blood-brain barrier at a rate of greater than 0.3, it may be able to do so with ease. The brain is significantly impacted by molecules, as evidenced by the pkCSM server's BBB permeability of -0.331. Another simple measurement obtained *via in situ* brain insertion, in which the medication is administered right into the carotid artery, is CNS permeability (log PS). According to the pkCSM prediction technique, compounds with log PS > -2 are thought to be capable of entering the central nervous system. The logPS value of -2.364 for the DBS molecule has been demonstrated to indicate its ability to enter the central nervous system [47]. It is believed that P-glycoprotein (P-gp) plays a part in the DBS molecule and its activation and suppression are both necessary for drug metabolism. The pkCSM server reports a total clearance rate of -0.014 when the molecule is used as a renal OCT2 substrate [48]. The acute and chronic toxicity limits of oral molecule treatment in rats were determined to be 2.303 (LD_{50}) and 0.954 (LOAEL), respectively. There is no suppression of hERG I or II [49] that the pkCSM server can find.

The lead drug DBS's efficaciousness, lipophilicity, solubility and boiled egg model were assessed using the free online program SwissADME [50]; the results are displayed in Table-9. If a ligand can pass through the blood-brain barrier (BBB), it can be demonstrated using the boiled-egg model. As to this research, the yellow part of the yolk symbolizes brain penetration, whereas the white, or albumin, component signifies gastrointestinal absorption. Fig. 8 shows that the drug component is located inside the yolk portion of the molecule's boiled egg model, which was generated by the SwissADME website. This indicates the blood-brain barrier-crossing capacity of the medicine. Only two hydrogen bond donors and acceptors are found in DBS, according to the results. One can use the fraction of sp^3 carbon atoms to forecast and characterize the solubility and aliphatic degree of medicinal molecules. A particular chemical's medicinal effectiveness rate may be increased by increasing its saturation as per some theories [51]. The DBS's fraction C sp^3 of 0.20 shown a substantial degree of saturation. Fig. 8 presents the generated radar map. The iLOGP, XLOGP3, WLOGP, MLOGP and SILICOS-IT had lipophilicity values

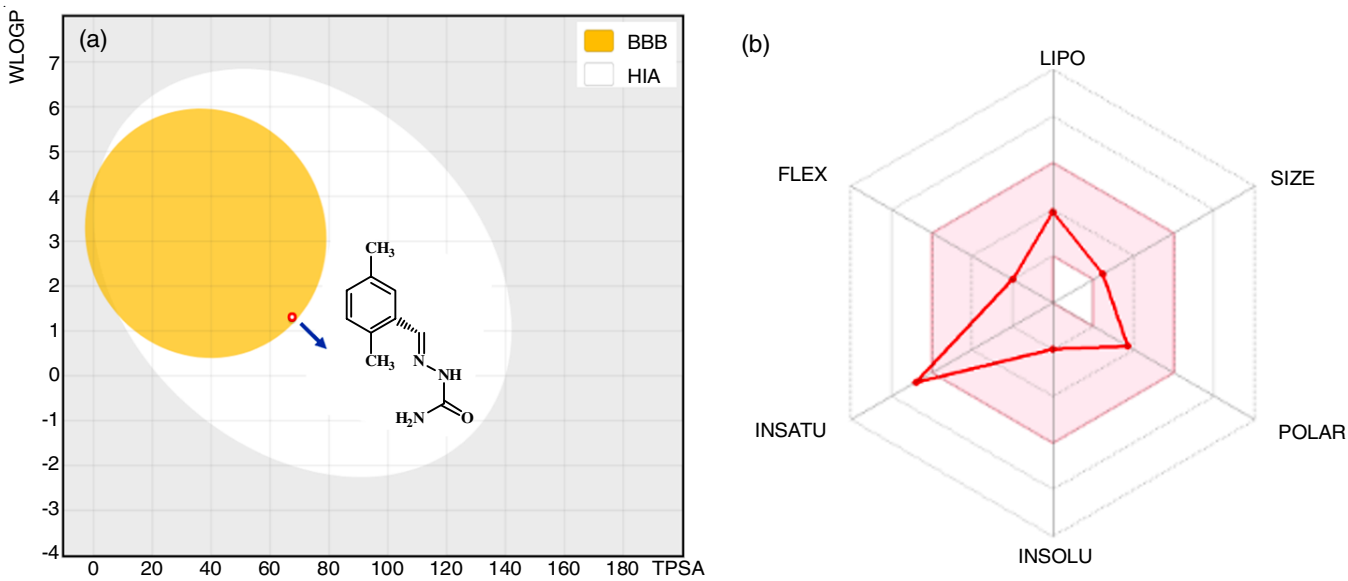

Fig. 8. (a) Boiled-Egg plot and (b) Radar plot of 2,5-dimethylbenzaldehyde semicarbazone

of 1.08, 1.33, 1.31, 1.69 and 1.50, respectively, according to the study. In that order, the water solubility values for ESOL, ALI and SILICOS-IT were -1.98, -2.35 and -2.91. Thus, DBS has been shown to meet all the criteria and be regarded as a potentially effective and safe medication, as indicated by these expected pharmacokinetic features.

Conclusion

Using the B3LYP/6-311++G(d,p) basis set computations, the ideal geometrical parameters, vibrational frequencies and vibrational intensities of the vibrational bands of 2,5-dimethylbenzaldehyde semicarbazone (DBS) were examined and compared with the experimental vibration values. The PED computation has yielded the most reliable theoretical evidence for the vibrational characteristics of the molecule. Mulliken's charge and HOMO-LUMO analysis were examined the electronic characteristics of the molecule and its molecular charge transfer interactions. As indicated by the oxygen and hydrogen atoms, the MEP analysis shows that the assaults are nucleophilic and electrophilic, respectively. According to the NBO results, there is a significant conjugative interaction between the molecules. The estrogen sulfotransferase receptor (PDB ID: 1AQU) has the highest binding affinity (-8.3 kcal mol^{-1}) and is the receptor that interacts with the DBS the most, based on docking studies. The physico-chemical and ADMET properties confirmed that DBS possesses drug-like qualities, indicating that the molecule is safe and complies with the Lipinski rules.

CONFLICT OF INTEREST

The authors declare that there is no conflict of interests regarding the publication of this article.

REFERENCES

1. A. Ahmad, *Adv. Exp. Med. Biol.*, **1152**, 1 (2019); https://doi.org/10.1007/978-3-030-20301-6_1
2. F. Bray, J. Ferlay, I. Soerjomataram, R.L. Siegel, L.A. Torre and A. Jemal, *CA Cancer J. Clin.*, **68**, 394 (2018); https://doi.org/10.3322/caac.21492
3. W. Cao, H.-D. Chen, Y.-W. Yu, N. Li, W.-Q. Chen and J. Ni, *Chin. Med. J.*, **134**, 783 (2021); https://doi.org/10.1097/CM9.0000000000001474
4. J. Zhang, Y. Wu, Y. Li, S. Li, J. Liu, X. Yang, G. Xia and G. Wang, *Phytomedicine*, **129**, 155600 (2024); https://doi.org/10.1016/j.phymed.2024.155600
5. M. Muthukkumar, T. Bhuvaneswari, G. Venkatesh, C. Kamal, P. Vennila, S. Armakoviæ, S.J. Armakovic, Y.S. Mary and C.Y. Panicker, *J. Mol. Liq.*, **272**, 481 (2018); https://doi.org/10.1016/j.molliq.2018.09.123
6. I.A. Mir, Q.U. Ain, T. Qadir, A.Q. Malik, S. Jan, S. Shahverdi and S.A. Nabi, *J. Mol. Struct.*, **1295**, 136216 (2024); https://doi.org/10.1016/j.molstruc.2023.136216
7. R. Maity, B. Manna, S. Maity, K. Jana, T. Maity, M. Afzal, N. Sepay and B.C. Samanta, *Inorganics*, **12**, 19 (2024); https://doi.org/10.3390/inorganics12010019
8. A. Ramalingam, S. Sambandam, M. Medimagh, O. Al-Dossary, N. Issaoui and M.J. Wojcik, *J. King Saud Univ. Sci.*, **33**, 101632 (2021); https://doi.org/10.1016/j.jksus.2021.101632
9. I. Jomaa, N. Issaoui, T. Roisnel and H. Marouani, *J. Mol. Struct.*, **1242**, 130730 (2021); https://doi.org/10.1016/j.molstruc.2021.130730
10. A. Sagaama, N. Issaoui, O. Al-Dossary, A.S. Kazachenko and M.J. Wojcik, *J. King Saud Univ. Sci.*, **33**, 101606 (2021); https://doi.org/10.1016/j.jksus.2021.101606
11. A.S. Kazachenko, Y.N. Malyar, N.Y. Vasilyeva, V.S. Borovkova and N. Issaoui, *Biomass Convers. Biorefin.*, **13**, 1004 (2021); https://doi.org/10.1007/s13399-021-01895-y
12. S. Bahceli, E.K. Sarýkaya and O. Dereli, *ChemistrySelect*, **9**, e202400054 (2024); https://doi.org/10.1002/slct.202400054
13. A. Ramalingam, C. Duraisamy, R. Ramarajan, A. Imojara, S. Sambandam, H. Louis and I. Benjamin, *J. Mol. Struct.*, **1299**, 137031 (2024); https://doi.org/10.1016/j.molstruc.2023.137031
14. A.D. Becke, *J. Chem. Phys.*, **98**, 5648 (1993); https://doi.org/10.1063/1.464913
15. A. Mishra, D. Sharma and S.N. Tiwari, *Indian J Pure Appl Phys.*, **61**, 810 (2023); https://doi.org/10.56042/ijpap.v61i9.3125
16. M. Raja, R. Raj Muhamed, S. Muthu and M. Suresh, *J. Mol. Struct.*, **1141**, 284 (2017); https://doi.org/10.1016/j.molstruc.2017.03.117
17. V. Latha, V. Gomathi and A. Rajeshkanna, *Indian J. Biochem. Biophys.*, **60**, 844 (2023); https://doi.org/10.56042/ijbb.v60i11.6067

18. M.J. Frisch, G.W. Trucks, H.B. Schlegal, G.E. Scuseria, M.A. Robb, J.R. Cheesman, V.G. Zakrzewski, J.A. Montgomerg Jr., R.E. Stratmann, J.C. Burant, S. Dapprich, J.M. Millam, A.D. Daniels, K.N. Kudin, M.C. Strain, O. Farkas, J. Tomasi, V. Barone, R. Cammi, B. Mennucci,M. Cossi, C. Pomelli, C. Adamo, S. Clifford, J. Ochterski, G.A. Petersson, P.Y. Ayala, Q. Cui, K. Morokuma, N. Rega, P. Salvador, J.J. Dannenberg, D.K. Malich, A.D. Rabuck, K. Raghavachari, J.V. Ortiz, J.B. Foresman, J. Cioslowski, A.G. Baboul, B.B. Stetanov, A. Liashenko, P. Piskorz, G. Liu, I. Komaromi, R. Gomperts, R.L. Martin, D.J. Fox, T. Keith, M.A. Al-Laham, C.Y. Peng, A. Nanayakkara, M. Challacombe, P.M.W. Gill, B. Johnson, W. Chen, M.W. Wong, J.L. Andres, C. Gonzalez, M. Head-Gordon, E.S. Replogle and J.A. Pople, GAUSSIAN 09, Revision A 11.4, Gaussian, Inc, Pittsburgh PA (2009).
19. R. Dennington, T. Keith and J. Millam, GaussView, Version 5, Semichem Inc., Shawnee Mission KS (2009).
20. M.H. Jamroz, Vibrational energy distribution analysis: VEDA 4 Program, Warsaw, Poland, (2004).
21. N.M. O'boyle, A.L. Tenderholt and K.M. Langner, *J. Comput. Chem.*, **29**, 839 (2008); https://doi.org/10.1002/jcc.20823
22. D. Seeliger and B.L. de Groot, *J. Comput. Aided Mol. Des.*, **24**, 417 (2010); https://doi.org/10.1007/s10822-010-9352-6
23. O. Trott and A.J. Olson, *J. Comput. Chem.*, **31**, 455 (2010); https://doi.org/10.1002/jcc.21334
24. U.P. Mohan, S. Kunjiappan, P.B. Tirupathi Pichiah and S. Arunachalam, *3 Biotech.*, **11**, 1 (2021); https://doi.org/10.1007/s13205-020-02530-9
25. S. Kim, P.A. Thiessen, E.E. Bolton, J. Chen, G. Fu, A. Gindulyte, L. Han, J. He, S. He, B.A. Shoemaker, J. Wang, B. Yu, J. Zhang and S.H. Bryant, *Nucleic Acids Res.*, **44(D1)**, D1202 (2016); https://doi.org/10.1093/nar/gkv951
26. S. Duklan, S. Saha, V. Jakhmola, N. Gairola, P. Pandey, M.P. Singh and S.M.A. Kawsar, *Adv. J. Chem. Sec. A*, **7**, 459 (2024); https://doi.org/10.48309/AJCA.2024.448978.1499
27. A. Daina, O. Michielin and V. Zoete, *Sci. Rep.*, **7**, 42717 (2017); https://doi.org/10.1038/srep42717
28. Y. Kia, H. Osman, V. Murugaiyah, M. Hemamalini and H.-K. Fun, *Acta Crystallogr. Sect. E Struct. Rep. Online*, **67**, o242 (2011); https://doi.org/10.1107/S1600536810052797
29. Y. Unal, W. Nassif, B.C. Ozaydin and K. Sayin, *Vib. Spectrosc.*, **112**, 103189 (2021); https://doi.org/10.1016/j.vibspec.2020.103189
30. S.L. Dhonnar, N.V. Sadgir, V.A. Adole and B.S. Jagdale, *Adv. J. Chem. A*, **4**, 220 (2021); https://doi.org/10.22034/AJCA.2021.283003.1254
31. E. Gobinath, S. Jeyavijayan, R.J. Xavier and J. Indian, *Pure Appl. Phys.*, **55**, 541 (2017).
32. S. Ramalingam and S. Periandy, *Spectrochim. Acta A Mol. Biomol. Spectrosc.*, **78**, 835 (2011); https://doi.org/10.1016/j.saa.2010.12.043
33. M. Karabacak, E. Sahin, M. Cinar, I. Erol and M. Kurt, *J. Mol. Struct.*, **886**, 148 (2008); https://doi.org/10.1016/j.molstruc.2007.11.014
34. N. Karthik, S. Jeyavijayan and S. Sumathi, *Indian J. Biochem. Biophys.*, **61**, 204 (2024); https://doi.org/10.56042/ijbb.v61i4.8236
35. C.S. Abraham, J.C. Prasana, S. Muthu, F. Rizwana B and M. Raja, *J. Mol. Struct.*, **1160**, 393 (2018); https://doi.org/10.1016/j.molstruc.2018.02.022
36. J.G. Malecki, *Polyhedron*, **29**, 1973 (2010); https://doi.org/10.1016/j.poly.2010.03.015
37. K. Parimala and V. Balachandran, *Spectrochim. Acta A Mol. Biomol. Spectrosc.*, **81**, 711 (2011); https://doi.org/10.1016/j.saa.2011.07.011
38. S. Uzun, Z. Esen, E. Koç, N.C. Usta and M. Ceylan, *J. Mol. Struct.*, **1178**, 450 (2019); https://doi.org/10.1016/j.molstruc.2018.10.001
39. N.A. Wazzan and F.M. Mahgoub, *Open J. Phys. Chem.*, **4**, 6 (2014); https://doi.org/10.4236/ojpc.2014.41002
40. S. Halder, P.C. Mandal, M. Guin and S. Konar, *J. Struct. Chem.*, **65**, 1 (2024); https://doi.org/10.1134/S0022476624010013
41. C. Morell, A. Grand and A. Toro-Labbe, *J. Phys. Chem. A*, **109**, 205 (2005); https://doi.org/10.1021/jp046577a
42. R. Singla, K.B. Gupta, S. Upadhyay, M. Dhiman and V. Jaitak, *Eur. J. Med. Chem.*, **146**, 206 (2018); https://doi.org/10.1016/j.ejmech.2018.01.051
43. S. Dettmann, K. Szymanowitz, A. Wellner, A. Schiedel, C.E. Müller and R. Gust, *Bioorg. Med. Chem.*, **18**, 4905 (2010); https://doi.org/10.1016/j.bmc.2010.06.016
44. S. Jeyavijayan, M. Ramuthai and P. Murugan, *Asian J. Chem.*, **34**, 2025 (2022); https://doi.org/10.14233/ajchem.2022.23677
45. D.E.V. Pires, T.L. Blundell and D.B. Ascher, *J. Med. Chem.*, **58**, 4066 (2015); https://doi.org/10.1021/acs.jmedchem.5b00104
46. S.N. Mali and A. Pandey, *J. Comput. Biophys. Chem.*, **20**, 267 (2021); https://doi.org/10.1142/S2737416521500125
47. Z. Ya'u Ibrahim, A. Uzairu, G. Shallangwa and S. Abechi, *Sci. Afr.*, **10**, e00570 (2020); https://doi.org/10.1016/j.sciaf.2020.e00570
48. F.A. Muslikh, E. Kurniawati, B. Maarif, S.Z. Zenmas, N. Salmasfattah, A.A. Dhafin and F. Prasetyawan, *Int. J. Contemp. Sci.*, **1**, 33 (2023).
49. M.A. Zolotovskaia, M.I. Sorokin, A.A. Emelianova, N.M. Borisov, D.V. Kuzmin, P. Borger, A.V. Garazha and A.A. Buzdin, *Front. Pharmacol.*, **10**, 1 (2019); https://doi.org/10.3389/fphar.2019.00001
50. K.A. Azzam, *Eng. Technol.*, **325**, 14 (2023); https://doi.org/10.31643/2023/6445.13
51. G. Aditya, C. Aman, S. Abhishek, D. Nanzeen, J. Swati, S. Nischal, G. Pratik and M. Rajesh, *Indian J. Biochem. Biophys.*, **59**, 848 (2022); https://doi.org/10.56042/ijbb.v59i8.62908